NeuroDeblur: A novel software for fast deconvolution of large light-sheet, confocal, or bright-field microscopy stacks.

Klaus Becker[1] & Saiedeh Saghafi[1]

[1]Meso-Aspheric Optics & LSFM, Institute of Solid State Electronics, Vienna University of Technology, Vienna, Austria.

Summary

We introduce *NeuroDeblur*, a groundbreaking deconvolution software that significantly enhances the visibility of intricate cellular details, including neurons, glia, and subcellular structures like axons and dendritic spines. The software offers non-blind deconvolution with a synthetic point spread function (PSF) optimized for each imaging mode, as well as the option to use a measured PSF. Originally developed for processing extremely large image stacks obtained from light-sheet microscopy, *NeuroDeblur's* advanced block-wise computational processing capabilities enable it to handle datasets of virtually unlimited size. Unwanted image background is removed using an advanced 3D rolling ball filtering algorithm. By leveraging parallelization and optional GPU acceleration on NVIDIA graphics cards, NeuroDeblur achieves remarkable processing speeds. For example, on a PC equipped with a mid-range gaming graphics card, a 3D stack containing approximately 1 billion voxels can be deconvolved within 5-10 minutes. This powerful combination of advanced features and efficient performance makes NeuroDeblur an indispensable tool for researchers seeking to unravel the intricacies of microscopic structures with unprecedented clarity and speed.

Methods

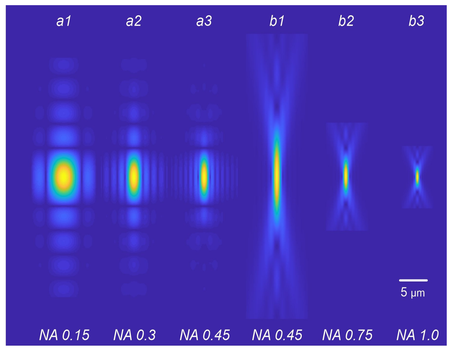

Figure 1: **Synthetic PSFs** for deconvolving confocal microscopy and light sheet microscopy data. (**a1-a3**) PSFs used for deconvolving light sheet microscopy data for three different objectives (*NA* = 0.15, *NA* = 0.3, and *NA* = 0.45). The assumed numerical aperture of the light sheet (NA_{Ls}) is 0.05. (**b1-b3**) PSFs used for deconvolution of confocal microscopy images for three different objectives (*NA* = 0.45, NA = 0.75, and NA = 1.0). Other parameters for all PSFs: Excitation wavelength = 488 nm, Emission wavelength = 520 nm, *n* = 1.56. To enhance the visibility of the side lobes of the PSFs, the images were gamma corrected by 0.4. For better visualization of the side lobes, the square root of the intensity (I) is plotted. The figure illustrates that the axial size of the PSF for a light sheet microscope mostly depends on NA_{Ls} and therefore is approximately independent of the numerical aperture of the objective. In contrast, the axial resolution of a confocal microscope massively decreases for low aperture objectives [1].

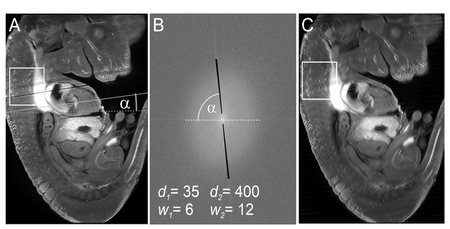

Figure 2: **Stripe artifact removal** in light sheet microscopy data using a directional frequency filter. **(A)** Representative slice of a data stack obtained from a cleared mouse embryo showing the stripe-shaped artifacts that typically occur in light sheet microscopy images. Frequently, these stripes are due to light-absorbing structures persisting through the chemical specimen clearing procedures applied in light sheet microscopy. By obstructing the light sheet, these structures produce shadows that form an angle α with the image edges. The position of the red line can be adjusted under visual control to measure the directional angle α of the stripes. **(B)** To remove these artifacts, the images are Fourier transformed and multiplied with a filter mask cutting out a pie-slice shaped segment of the spectrum that matches the angular direction α of the stripes. **(C)** After inverse transformation and rescaling, an improved image with less visible stripes is obtained [2].

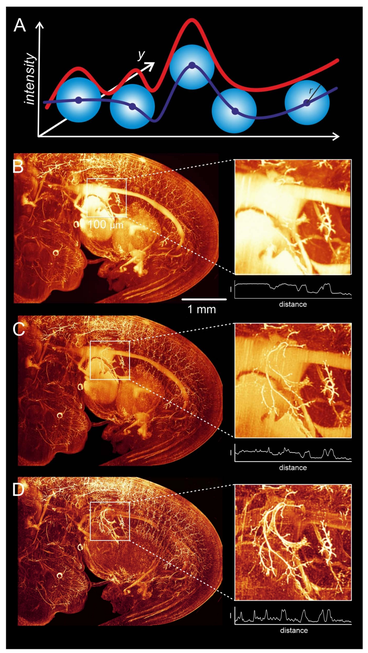

Figure 3: Example of **rolling ball filtering**. **(A)** Any grayscale image can be represented as a 3D-profile by plotting the luminance values along the vertical axis of a 3D coordinate system. A virtual ball with radius r rolling along the lower side of this profile would fit more or less into the "cavities" of the 3D surface, depending on the radius r. Connecting all possible locations of the center of the ball defines a smoothed profile that represents the image background. This background is subtracted from the original image to obtain the processed image. For processing 3D stacks we apply the rolling filter successively to all *xy*-, *xz*-, and *yz*-planes in the stack. **(B)** 3D reconstruction obtained from a chemically cleared, immune stained E12.5 mouse embryo. The 3D reconstruction was obtained using 667 slices recorded with a 2.5x objective (Zeiss FLUAR 2.5x, Carl Zeiss, Germany, NA 0.12). **(C)** 3D reconstruction obtained after deconvolution without rolling ball background removal. **(D)** Deconvolution obtained after rolling ball filtering with *r* = 75 µm and subsequent deconvolution with the same parameters as in (C). The increase in visibility of details is obvious, especially from the marked details [3].

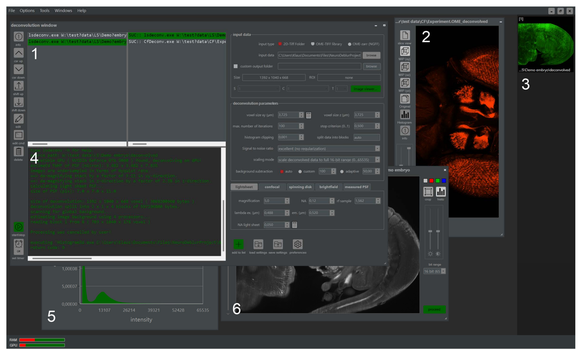

Figure 4: *NeuroDeblur* offers an easy-to-use **graphical user interface (GUI)** for deconvolving light sheet, confocal, and brightfield microscopy data. Additionally, the GUI provides many additional features such as timer-controlled batch processing, visualization of the deconvolved data, and post-processing using different filters. As an alternative to using the GUI, *NeuroDeblur* also offers a collection of separate command line tools for working within a console window. This design allows for easy embedding of deconvolution into complex workflows via script files, e.g., written in Python. **(1)** The 'deconvolution window' for setting deconvolution parameters and various options. **(2)** The 'result window' displays the deconvolution results and provides options for visualization (e.g., MIP) or comparing the deconvolution results with the raw data in synchronized windows. **(3)** 'Preview area' where preview images of the deconvolved data sets are displayed. **(4)** Console window for showing the progress of the current deconvolution task as well as warning and error messages. **(5)** The 'Histogram window' allows displaying a histogram of an input stack to check data sets for over-exposure or unwanted clipping. **(6)** The 'Region editor' allows the definition of regions of interest (ROIs) in the raw data or the selection of distinct image channels or points of time in supported image formats such as OME-tiff.

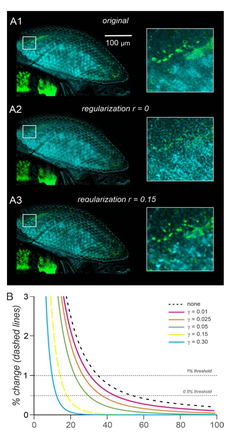

Figure 5: Our deconvolution algorithm uses **flux-preserving regularization** instead of Tikhonov-Miller or Total Variation Regularization, as in most other deconvolution algorithms. To our knowledge, this approach has been used in astronomy but has never been applied to deconvolving microscopy data before. A major strength of flux-preserving regularization is the strict preservation of the total photon flux. This means that the intensity values are only redistributed, with no extra 'light' added or removed from the image stack due to the deconvolution process. This preservation of photometry is an important prerequisite for performing exact quantifications of fluorescence intensities among multiple image stacks or regions of interest within the same stack.

Results

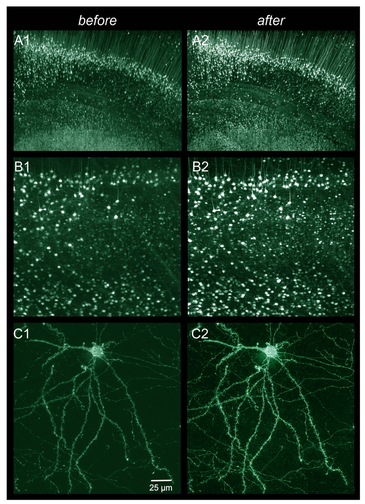

Figure 6: A-B: Cortical neurons in a entire chemically cleared mouse brain. Labeling: Thy1-eGFP. Excitation wavelength: 488 nm, Imaging system: ClearScope Light Sheet Theta Microscope (mbf Bioscience, USA) Objective: 10x NA 0.6 (Olympus XLPLN 10x SVMP). Emission Filter: Chroma ZET405/ 488/561/640mv2. **C: Cortical neurons in a 30 µm thick brain slice.** The neuron is a cortical pyramidal neuron that projects to the Cholinergic (ChAT) neurons in the striatum using the modified rabies retrograde transsynaptic tracing technique. Injection of an AAV-Helper virus with a Cre-dependent construct to express TVA in ChAT neurons expressing CRE in the striatum was followed with an injection into the same striatal site EnvA-rabies EGFP virus, which selectively infects striatal ChAT neurons (that express TVA following the AAV-helper injection) and is transynaptically retrogradely transported to cortical neurons. Labeling RFP. Excitation wavelength: 555 nm. Imaging system: Vesalius spinning disc microscope (mbf Bioscience, USA). Objective: 40x NA 0.75 (Zeiss, Germany). Emission filter: Chroma ZET 405/470/555/640/730m_OD8.

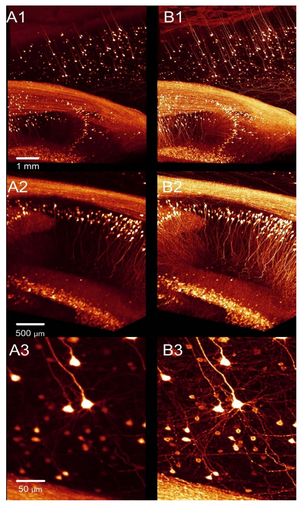

Figure 7: Hioopcampal neurons recorded from an entirely cleared mouse brain before and after deconvolution. Imaging was done using a light sheet microscope equipped with a custom light sheet generator providing a high Rayleigh range (*NA* = 0.05) (Objective: Zeiss FLUAR 4x, *NA* 0.28, 2x post magnification). **A1-A3:** 3D reconstructions obtained from the raw data: *MIP* obtained from 777 slices with 2560 x 2160-pixel resolution, recorded with an Andor Neo CCD camera (Oxford Instruments, Germany). **B1-B3:** 3D reconstructions obtained from the same data as in (A) but after deconvolution. Deconvolution parameters: *NA* = 0.3, λ_{ex} = 488 nm, emission λ_{em} = 520 nm, *n* = 1.561, NA_{LS} = 0.04, stop criterion = 0.2%, max. iterations = 100, histogram clipping = 0.01, no regularization, no background subtraction.

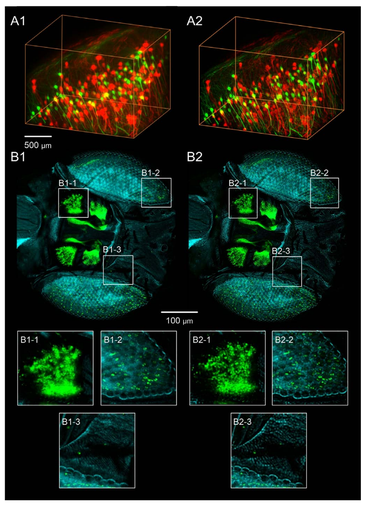

Figure 8: Deconvolution of multi-channel images. (A) Double staining of neurons in the mouse hippocampus before and after deconvolution. Imaging was done using a light sheet microscope equipped with a custom light sheet generator (NA_{LS} = 0.05). Imaging was performed with a 25x objective NA = 1.0 (Olympus XLSLPLN25XGMP) **A1**: Raw data: Maximum intensity projection obtained from 2 x 786 slices with 2560 x 2160-pixel resolution, recorded with an Andor Neo CCD camera (Oxford Instruments, Germany). **A2:** Reconstruction obtained from the same data set after deconvolution. The increase in sharpness after deconvolution is evident. Deconvolution parameters: NA = 1.0, excitation wavelengths: λ = 488 nm, λ = 532 nm, emission wavelengths: λ = 520 nm, λ = 560 nm, *n* = 1.561, NALs = 0.05, stop criterion = 0.5%, max. iterations = 100, histogram clipping = 0.01, no regularization, rolling ball filter radius *r* = 15 µm. **(B1)** Reconstructions of the faceted eye of a fruit fly before and after deconvolution. The 2-channel confocal microscopy images were obtained using neuronal staining (channel 1) and autofluorescence (channel 2). Objective: 25x NA 0.7. **B1:** Maximum intensity projection obtained from the raw data (2 x 69 slices with 1024 x 1024-pixel resolution, 2 channels λ_{ex} = 488, 626 nm and λ_{em} = 532, 560 nm). **B2:** Reconstruction obtained after deconvolution. The improvement in sharpness and level of detail is obvious. Deconvolution parameters: *NA* = 0.7, λ_{ex} = 488, 523 nm and λ_{em} = 526, 560 nm, *n* = 1.45, pinhole diameter = 0.75 AU, stop criterion = 0.5%, max. iterations = 100, histogram clipping = 0.01, regularization = 0.1, no background subtraction.

References: 1. Becker, K., Saghafi, S., Pende, M., Sabdyusheva-Litschauer, I., Hahn, C., Foroughipour, M., … Dodt, H.-U. (2019). Deconvolution of light sheet microscopy recordings. Scientific Reports, 9(1), 1–14. https://doi.org/10.1038/s41598-019-53875-y. **2.** Sabdyusheva Litschauer, I., Becker, K., Saghafi, S., Ballke, S., Bollwein, C., Foroughipour, M., … Dodt, H. U. (2020). 3D histopathology of human tumors by fast clearing and ultramicroscopy. Scientific Reports, 10(**1**). https://doi.org/10.1038/s41598-020-71737-w. **3.** Visualizing minute details in light-sheet and confocal microscopy data by combining 3D rolling ball filtering and deconvolution. Journal of Biophotonics, (October), 1–16. https://doi.org/10.1002/jbio.202100290.